Article

Wound Healing Potential of Plant Secondary Metabolites: *In Silico, In Vitro,* and *In Vivo* Experiments

Omar Casadiego[1], Oscar Macias[1,2], Laura García[1], Elkin Sanabria-Chanaga[3], J. Baay Guzmán[4], Julio Cesar Mantilla[5], and Patricia Escobar[1,*]

[1] Centro de Investigaciones en Enfermedades Tropicales, Escuela de Medicina, Universidad Industrial de Santander. Piedecuesta 681011, Colombia; o.casadiego@hotmail.com, lauragarcia952@gmail.com
[2] Semillero de Investigación en Enfermedades Tropicales (SINAT), CINTROP, Escuela de Medicina, Universidad Industrial de Santander. Piedecuesta 681011, Colombia
[3] Facultad de Ciencias Básicas, Departamento de Química, Universidad de Pamplona, Norte de Santander, Colombia; elkin.sanabria@unipamplona.edu.co
[4] Unidad de investigación en enfermedades Oncológicas, Hospital Infantil de México: Federico Gómez, México DF, México; guillebaay@gmail.com
[5] Departamento de Patología, Escuela de Medicina, Universidad Industrial de Santander, Bucaramanga, Colombia; jumantil@uis.edu.co
* Correspondence: e-mail pescobar@uis.edu.co

Abstract: Dysregulation of the arsenal of cells, growth factors, cytokines, proteases, and proteins involved in wound healing (WH), could delay the healing process. Plants and plant-derived molecules (PDMs) have been used as medicines for skin wounds. This study aimed to select and evaluate the pro-healing capacity of PMDs. Thirty-three PDMs and 10 therapeutic targets (TTs) were chosen for molecular docking and PDMs: aristolochic acid (AA), α-copaene, selinenes, β-caryophyllene (BC), and BCoxide, and TTs: metalloproteinase (MMP) 3, MMP13, and tumor necrosis factor (TNF α) for molecular dynamics. The bests inhibitor was AA, but because of its toxicity, BC and BCoxide were chosen for evaluation in HaCat cells and BALB/c mice excisional model. Both compounds were not toxic, and higher percentages of lesion area closure (LAC) were induced by BC treatment ($p<0.05$). All mice healed; however, an initial delay of LAC was induced by 0.05, 0.1% BCoxide, 0.1% BC, and allantoin. At the end of treatment, lower numbers of mast cells, level of cellular infiltrates (except 1% BCoxide and 0.05, 0.5%BC), epidermal thickness tendency (except 0.1, 0.5% BCoxide), and higher values of SC-thickness, and collagen fibers only by 0.5% BC treatment compared with untreated control ($p<0.05$) were observed. Our results show that BC is a promising multitarget candidate for wound healing treatment and optimization campaigns.

Keywords: wound healing; natural compound; excisional mouse model; molecular docking; dynamic molecular; caryophyllene; cytokines; digital histology

1. Introduction

The wound healing (WH) process consists of four overlapping phases: hemostasis (0–several hours after injury), inflammation (1–3 days), proliferation (4–21 days), and remodeling (21 days–1 year) [1]. Initially, there is vasoconstriction, platelets activation, and the formation of a fibrin/fibronectin-rich provisional extracellular matrix (ECM) clot, and a release of growth factors (GF) including tissue GF (TGFβ1), platelet-derived GF (PDGF), fibroblast GF (FGF), and epidermal GF (EGF), and pro-inflammatory cytokines e.g., TNFα, IL6, and IL-1β [1]. Damage and pathogen-associated patterns, and chemoattractant as monocyte chemoattractant protein MCP1/CCL2 drive the recruitment of neutrophils, monocytes/macrophages, lymphocytes, and mast cells. Macrophages release pro-inflammatory cytokines, reactive oxygen, and nitrogen species and differentiate into anti-inflammatory, pro-vascular, and profibrotic macrophages which release vascular endothelial GF (VEGF), PDGF, TGFβ1, IL-10, and ECM deposits for scar formation and organization [3]. In the proliferative phase, endothelial cells migrate toward the wound and started angiogenesis in response to pro-angiogenic signals such as VEGF, endothelial GF (EGF), PDGF, and TGFβ. Fibroblasts migrate

Preprints (www.preprints.org) | NOT PEER-REVIEWED | Posted: 20 April 2023 doi:10.20944/preprints202304.0619.v1

along the fibrin network, proliferate, and transform into myofibroblasts promoting the formation of granulation tissue by synthesizing ECM, matrix metalloproteinases (MMPs), and tissue MMPs inhibitors (TIMPs) [4]. For reepithelization, keratinocytes released from the wound edge, migrate, proliferate, and release ECM with the help of epidermal and fibroblast GF including EGF, TGFα, FGF2, or KGF and upregulate keratin production. For wound remodeling, the granulation tissue is replaced with a scar or normal connective tissue (collagen I), and there is a regression of the neo-vasculature, synthesis of MMPs, and TIMP by myofibroblasts [5].

However, a complete or scar-less WH will not always occurs. Some wounds, heal in a prolongated, and unpredictable period (chronic wounds, CW) characterized usually by excessive inflammation, enhanced proteolysis, impaired re-epithelization, matrix deposition, and collagen synthesis between others [6,7]. CW prevalence increases each year, and the treatment becomes more complicated and expensive [6,7]. Currently, ionizing radiation, chemical products, wound dressings, or advanced therapies, including extracellular matrices, growth factors, and negative pressure are used, however, they are expensive, require long hospitalization times, and their efficacy is variable depending on the etiology, and individual characteristics [7]. The search for new therapies to improve both the acute and CW healing process using different *in silico*, *in vitro, ex-vivo,* and *in- vivo* approaches, goes on. Different tools using computational devices are available to evaluate the pharmacological properties and binding capacities of small bioactive candidates on pivotal targets of the healing process [8]. Some plant extracts and their plant-derived molecules (PDMs) e.g., *Vasconcellea cundinamarcen*sis or papayuela (Pycnogenol®), *Calendula officinalis* L. (faradiol-3-O-myristate), *Symphytum* × *uplandicum* Nyman (allantoin), *Aloe vera* (acemannan) have been evaluated in clinical trials on patients with diabetic foot ulcers, pressure ulcers, or venous legs ulcers with very promissory results [9]. To contribute to the search for new pro-healing compounds, this study aimed to determine the WH potential of different PDMs, more of them included in essential oil distilled from aromatic Colombian plants. The inhibitory interaction of 33 PDMs with 10 therapeutic targets (TTs) was studied by molecular docking, and 6 of the best candidates were selected and evaluated by molecular dynamics against 3 TTs. The two best candidates were evaluated for cytotoxicity, proliferation/migration, and wound-healing activity in a BALB/c mice excisional model.

2. Materials and Methods

2.1 Plant-derived metabolites (PDM)

The 33 PDMs (table 1) analyzed were selected based on their structure availability in the databases used: Drug Bank (www.drugbank.ca) and PubChem (https://pubchem.ncbi.nlm.nih.gov).

Table 1. Secondary plant-derived metabolites used in screening. Bold letters mean data obtained from Data Bank. The others were from the PubChem database.

ID Code	Ligand Name	ID Code	Ligand Name
2236	Aristolochic acid	**11672**	**Curcumin**
15573	**α-Pinene**	8815	Estragole
70678558	α-Copaene	2758	Eucalyptol
5281520	α-Humulene	**09086**	**Eugenol**
7460	α-Phellandrene	**7461**	**γ-Terpinene**
10856614	α-Selinene	6549	Linalool
10545	Ascaridole	31253	Myrcene
5281515	(E)-β-caryophyllene	319084028	1,6-Octadiene
11142	β-Phellandrene	71742210	Caryophyllene oxide
14896	β-Pinene	7463	ϱ-Cymene
442393	β-Selinene	439570	(R)- (-)-Carvone
7001	1-Bromonaphthalene	16724	(S)- (+)-Carvone
01744	**Camphor**	440917	R-Limonene
10364	Carvacrol	439250	S-Limonene
6616	Camphene	18818	Sabinene
5320128	*cis*-Nerolidol	**02513**	**Thymol**
7794	Citronellal		

Preprints (www.preprints.org) | NOT PEER-REVIEWED | Posted: 20 April 2023 doi:10.20944/preprints202304.0619.v1

2.2 *Therapeutic targets (TTs)*

Ten (10) TTs were selected based on their key role in WH phases, accessibility of native ligand or inhibitor, presence in the protein data bank (PDB), and quality of the X-ray crystal structure (Table 2).

Table 2. Therapeutic targets used in screening. The grid size (x, y, z) was 40 x 40 x 40 except for IL-6 which was 50 x 50 x 50.

ID PDB	Therapeutic target	Coordinates (x, y, z)
2AZ5	Tumor necrosis factor-α (TNFα)	-19.259, 74.79, 34.032
1ALU	Interleukin-6 (IL6)	-3.934, -18.113, 3.394
5IKQ	Cyclooxygenase-2 (COX2)	22.222, 52.346, 18.018
4OEE	Fibroblast growth factor-2 (FGF2)	-11.744, -6.027, -3.03
1Q5K	Glycogen synthase kinase-3β (GSK3β)	23.992, 22.827, 8.884
2ZM3	Insulin-like growth factor 1 (IGFR1)	37.061, 79.097, 58.051
2D1O	Matrix metalloproteinases (MMP3)	28.762, 6.733, 14.320
1GKC	MMP9	48.145, 64.140, 42.896
2PJT	MMP13	9.323, 27.639, 141.777
3HNG	Vascular endothelial growth factor receptor-1 (VEGFR1)	4.729, 17.729, 33.352

*Each point equals 0.375

2.3 *Co-crystallized ligand*

The native ligand structures of each TT were obtained by removing all water molecules and heteroatoms from the target protein structure using BIOVIA Discovery Studio Visualizer software.

2.4 *Ligand and target interaction*

For PDMs and co-crystallized ligand mechanical force field (MMFF94), calculations were performed using Avogadro® open license software version 1.2.0 for Windows. Auto-Dock Tools version 1.5.6 (a graphical user interface program) was used for therapeutic target preparation. Kollman unified atomic charges, solvation parameters, and polar hydrogens were added to the receptor for protein preparation [10]. The structures of native ligands docked at one position were marked as the active site and the grid box size and center grid position was determined using the grid box coordinates shown in Table 2.

2.5 *Molecular Docking Analysis*

Molecular docking was performed using Autodock 4.2 software [10] using a genetic algorithm with a population size of 150 and a Lamarckian algorithm as the output parameter as the local search mechanism. Files were obtained in .dlg format to calculate the binding free energy (ΔG) and the inhibitory constant (Ki). Results were expressed as ΔG (kcal/mole) and Ki (μM). The results were averaged and compared by statistical test (Kruskal-Wallis test) and with the co-crystallized ligand (Dunn's test).

2.6 *Selection of best candidates*

Taking into consideration the ΔG and Ki values between the co-crystalized ligand (natural ligand) and each TT interaction, compounds were compared with the co-crystalized ligand (natural ligand) and classified as compounds with lower ΔG, equal ΔG, and equal Ki, equal ΔG and lower Ki, and higher ΔG. The compounds with lower ΔG compared to the co-crystallized ligand displayed the highest level of interaction with the target.

2.7 *Molecular dynamics (MDs) simulations*

The MD simulation, a modified protocol implemented in previous work [11] was performed using GROMACS 2018.2 installed in NMRbox server [12]. The lowest ΔG conformation of each

Preprints (www.preprints.org) | NOT PEER-REVIEWED | Posted: 20 April 2023 doi:10.20944/preprints202304.0619.v1

selected complex was considered the initial conformation for MD studies. Parameters and molecular topologies for the ligands were generated using the semi-empirical quantum chemistry program (SQM) of the AnteChamber PYthon Parser interface (ACPYPE). Complexes were described using the all-atom Amber99-ILDN force field. Protein-ligand complex was solvated with water on all sides using a three-point model for water (TIP3P) and 0.15 M NaCl solution additionally. Energy minimization was performed using the steepest-descent algorithm. The system was equilibrated with a constant-temperature-volume (NVT) and constant-temperature-pressure (NPT) ensemble with Berendsen thermostat and Parrinello- Rahman barostat respectively. A 100 ns MD simulation was performed on the protein-ligand complex. The root-mean-square deviation (RMSD) was analyzed during the complete MD simulation and ΔG of the complex based on the molecular mechanics Poisson-Boltzmann surface area (gmx_MMPBSA) calculations [13].

2.8 In vitro tests

2.8.1 *Cell line*

The human keratinocyte cell line (HaCat) was kindly provided by Sandra Leal Pinto PhD-Universidad de Santander. The cells were cultured in a DMEM medium (Gibco, NY, USA) supplemented with 10% fetal calf serum (FCS) (Gibco).

2.8.2 *Resazurin assay*

Cells (5 x 10^5 cells/ml) were seeded into 96-well plates for 24 h in a culture medium, and treated with serial concentrations of PDMs (4.7-300 μg/mg) at 37 °C for 72 h. After treatment, 20 μL of resazurin (0.1 mg/mL) was added to each well and after 4 h, the absorbance was measured spectrophotometrically by using a Synergy H1 plate reader (BioTek, Vermont, USA) at 570 and 600 nm. The cytotoxic concentrations 50 (CC_{50}) were calculated by non-linear regression (sigmoid) using XLfit® software (Business Solution, Guildford, UK). All experiments were conducted in triplicate.

2.8.3 Scratch wound migration assay

HaCat cells onto 12-well plates at 85-90% confluence were scratched with a 100 μL micropipette tip, washed twice with culture medium, and incubated with or without PDMs, allantoin, and 10% FCS in medium supplemented with 1.5% FCS. Cell migration from the basal line was microscopically detected at 24 h posttreatment. Images were captured using a light microscope (400x magnification). The percentage of occlusion was calculated from the open area in pixels with the aid of the ImageJ software (NIH, MD, USA).

2.9 In vivo experiments

2.9.1 Animals and ethical considerations

BALB/c mice (6-8 weeks) were supplied by the National Health Institute (Bogota, Colombia) and housed with a 12h light/dark cycle, 22 °C ± 2 °C, 55%+5% relative humidity with access to water and mouse food pellets ad libitum. All protocols were approved by the Industrial University of Santander (Bucaramanga, Colombia) Ethics Committee (Number 4110) causing minimal suffering in the animals.

2.9.2 Formulation preparation

Formulation (w/w) of 0.5 and 1.0% allantoin, 0.05, 0.1 0.5, 1% β-caryophyllene oxide (BCoxide), 0.05, 0.1, 0.5 and 1% β-caryophyllene (BC) and vehicle (without compound) were prepared in phosphate-buffered saline (PBS, pH 7.4) and 20% Kolliphor® (BASF Pharma, New Jersey, USA). Actives compounds were purchased from Sigma-Aldrich, St Louis, USA.

Preprints (www.preprints.org) | NOT PEER-REVIEWED | Posted: 20 April 2023 doi:10.20944/preprints202304.0619.v1

2.9.3 Wound model

After shaving, two circular excision wounds were made on each side of the dorsal region using a 5 mm punch biopsy under anesthesia. Mice (n = 7) were treated daily with BCoxide, BC, allantoin, and vehicle formulations directly to each wound, for 10 days. Untreated mice were used as control. Mice were sacrificed six hours after the last treatment using a Ketamine/Xylazine mixture. The n of mice (power 80% and alpha 0.05) was calculated from a pilot test (n = 3) using G*power software. Digital photographs were evaluated using ImageJ software. A yellow 1 x 2 cm sticker near the lesion was used as a guide. The wound (W) area was calculated for each time point, and the percentage of wound closure by the formula: % W closure = (initial W area – final W area)/initial W area x 100. Areas under the curve (AUCs) were calculated from the lesion sizes over the 10 days of the experiments [14].

2.9.4 Histological analysis

After 10 days of treatment wound samples were excised, fixed with 10% formalin for at least 24 h, embedded in paraffin and sectioned in 5 μm. Samples from normal skin were processed equally. Slides were stained with hematoxylin-eosin (H-E), toluidine blue (TB), and Masson's trichrome (MT) stains. The stained tissues were digitized using the Aperio ScanScope-CS2 (Leica Biosystems, Deer Park, United States) at 40x magnification. The .svs file was analyzed using Image Scope (Aperio) software. Mast cell and inflammatory infiltrates (cell numbers/microscopic field at 40x) were determined in TB and H-E staining, respectively. The thickness (μm) of the epidermis (excluding-stratum corneum, SC) and SC were quantified in HE-stained tissues. Quantification of collagen was performed in MT staining tissues by calculating the total intensity and number of blue-positive pixels per area (mm^2).

2.9.5 Tissue-protein and IL-6, IL-1 β, VEGF, and TNFα determination

Wound samples were homogenized in PBS pH 7.0, containing 0.2% Triton X-100, and protease inhibitors (SIGMAFAST™ Tablets, Sigma) using Ultraturrex. Tissue debris was cleared by centrifugation at 10000 g for 20 min. The total protein concentration was measured using a BCA Protein Assay kit (BIO BASIC, NY, USA), and the tissue levels of cytokine and VEGF using a commercial ELISA kit (R&D Systems Promega, Madison, WI, USA) following the manufacturer's recommendations.

2.9.6 Statistical analysis

Graphs and statistical analyses were performed using Prism software version 8.0.0 for Windows (San Diego, California, USA). The Kolmogorov-Smirnov test was used to determine normality. Analysis of variance (ANOVA) was used as a parametric test and the Kruskal-Wallis test as a non-parametric test. In both cases, Dunett's multiple comparisons were used. The following levels of significance were used p <0.05 (*), p <0.01 (**) and p <0.001(***).

3. Results and discussion

3.1 PDMs versus recognized inhibitors of WH-targets

Based on the statistical comparisons between PDMs and the co-crystallized ligands for each TT (Figure 1), the PDMs selected (those to displayed lower ΔG interactions compared to the co-crystallized ligand) were seven: aristolochic acid (AA) with two interactions (TNFα and COX2), α-copaene with three (TNFα, MMP13, and MMP3), α-humulene with one (TNFα), α-selinene with two (TNFα and MMP3), ascaridole with one (TNFα), β-caryophyllene (BC) with three (TNFα, MMP-13, and MMP3), β-selinene with three (TNFα, MMP13, and MMP3), and caryophyllene oxide (BCoxide) with four (TNFα, COX2, MMP13, and MMP3). The TTs with the higher number of lower ΔG interactions were TNFα > MMP3 > MMP13 > COX2 with 8, 5, 3, and 2 PMDs respectively. In contrast, the TTs with the higher number of higher ΔG interactions in descendent order were IGFR1= FGF-2 >

 doi:10.20944/preprints202304.0619.v1

GSK3ß > MMP-9 > COX-2 > MMP13 > IL-6 > MMP3 > VEGFR1 with 33, 33, 31, 30, 24, 10, 9, 5, and 4 PMDs respectively. PDMs such as estragole, γ-terpinene, linalool, and 1,6-octadiene displayed higher ΔGs with 8 TTs interactions and myrcene with 9.

Previous works have demonstrated the healing activities of some of our chosen PDMs, pure or as major plant extract components. In the case of AA, it can inhibit phospholipase A2 blocking the release of arachidonic acid from the cell membrane, a precursor of prostaglandins, a recognized pro-inflammatory-lipid mediator catalyzed by cyclooxygenases (COX-1 constitutive, COX-2 inducible) [13]. Some *Aristolochia* extracts increased fibroblasts and keratinocytes migration, collagen type-1 production, inhibited lipopolysaccharide (LPS)-induced nitric oxide (NO), IL-1β, and iNOS [16,17], and in rats, induced an increase of wound contraction, collagen, and production of some antioxidant enzymes [18]. For α-copaene, topical treatment of *Copaifera paupera* oleoresin (22.9% α-copaene and BC) improved WH in diabetic mice, induced downregulation of TNFα and MCP-1, upregulation of IL-10 (an anti-inflammatory cytokine) and induced higher levels of collagen and indexes of re-epithelialization [14]. Essential oil from *Ageratum fastigiatum* (containing α-copaene, BCoxide, α-humulene, and BC) reduces integrin β2 (CD18) expression and TNFα production on PMA-activated human lymphocytes or neutrophils [17]. Topical treatment with an ointment containing 4% EO extracted from *Cinnamomum verum* (12.3% α-copaene) decreases bacterial infection, displayed a faster inflammatory phase, promotes keratinocyte and fibroblasts migration/proliferation, angiogenesis, re-epithelialization, and collagen and keratin biosynthesis in mice infected excisional model [20]. For selinenes, formulations contained EOs from *Piper gaudichaudianum* contains β-selinene (14.0% and BCoxide 9.3%) inhibits neutrophil chemotaxis [21] and from *Helichrysum italicum* contained 11.0% β-selinene and 7.3% α-selinene decreased wound size and showed higher values of hydroxyproline content on diabetic rats [20]. Finally, some of the most studied and promising compounds are the related sesquiterpenes α-humulene, BC, and BCoxide, their oxidized form. For α-humulene (called also α-caryophyllene), topical treatment with Acheflan® cream (0.5% *Cordia verbenacea*-EO and 2.5% α-humulene) in rat excisional wounds induced a complete remodeling of the epidermis with increased levels of hydroxyproline, and collagen distribution. Increased levels of VEGF and MMP-9 were induced by day 8th, but a slight decrease at 15 days [23]. *Eugenia dysenterica*-EO (BC 24.4%, α-humulene 19.3%) stimulates fibroblast migration, decreases LPS-induced NO release on macrophages, and promotes a proangiogenic response on chick embryo chorioallantoic membranes [24]. Like BC, BCoxide contained in EO or pure exhibit anti-inflammatory, antioxidant, and analgesic activities affecting additionally growth and proliferation of numerous cancer cells [25].

Preprints (www.preprints.org) | NOT PEER-REVIEWED | Posted: 20 April 2023 doi:10.20944/preprints202304.0619.v1

Figure 1. Heat map of the classification of the interaction levels of the PDMs with the therapeutic targets (TT). Higher color intensity implies better interaction compared to the interaction obtained for the co-crystallized ligand.

3.2 Molecular dynamics between PDMs inhibitors and MMP-3, MMP-13, and TNFα targets

The PDMs AA, α-copaene, α-selinene, BC, β-selinene, and BCoxide, and their possible targets MMP-3, MMP-13, and TNFα were chosen for MD simulations. Following the binding free energy values, all the PDMs tested displayed interaction with MMP-3, MMP-13, and TNFα, except BCoxide with MMP-3 (Table 3). Interestingly, the interaction of AA with MMP-3 and MMP-13 was even much higher than that of the natural ligand. None of the PDMs surpassed reference ligand- TNFα interaction (Table 3).

Preprints (www.preprints.org) | NOT PEER-REVIEWED | Posted: 20 April 2023 doi:10.20944/preprints202304.0619.v1

Table 3. Binding free energy values for each target-ligand complex (mean +/- standard deviation). Based on the dynamics of MMP-3, MMP-13, and TNFα with their respective co-crystallized ligand and PMDs. *: $p < 0.05$

Ligand	Target		
	MMP-3	**MMP-13**	TNFα
Co-crystallized ligand	-51.755 +/- 4.118	-29.563 +/- 3.255	-48.432+/- 3.139
Aristolochic acid	-57.820 +/- 5.573*	-56.075 +/- 5.712*	-25.796+/- 2.176*
α-Copaene	-17.447 +/- 1.967*	-21.081 +/- 2.193*	-26.874 +/- 2.083*
α-Selinene	-28.741 +/- 2.063*	-20.222 +/- 4.226*	-19.417 +/- 1.808*
β-Caryophyllene	-17.432 +/- 2.554*	-23.419 +/- 2.948*	-26.386 +/- 1.686*
β-Selinene	-17.107 +/- 2.168*	-24.646 +/- 2.489*	-24.303 +/- 2.188*
Caryophyllene oxide	no interaction	-27.980 +/- 1.989*	-25.709 +/- 2.216*

Regards the MMPs-PDMs simulations, for the MMP-3 pocket, AA and α-selinene displayed the best behavior (like co-crystallized ligand), α-copaene, BC, and β-selinene displayed continuous fluctuation and BCoxide moved out of the pocket after 50 ns (Figure 2a and 2b). For MMP-13 (Figure 2c), satisfactory behaviors were displayed by AA, and BCoxide, stable conformations (but mostly at the end of the simulation) by α-copaene, BC, and β-selinene, while α-selinene showed an unstable fluctuation in the last 10 nanoseconds.

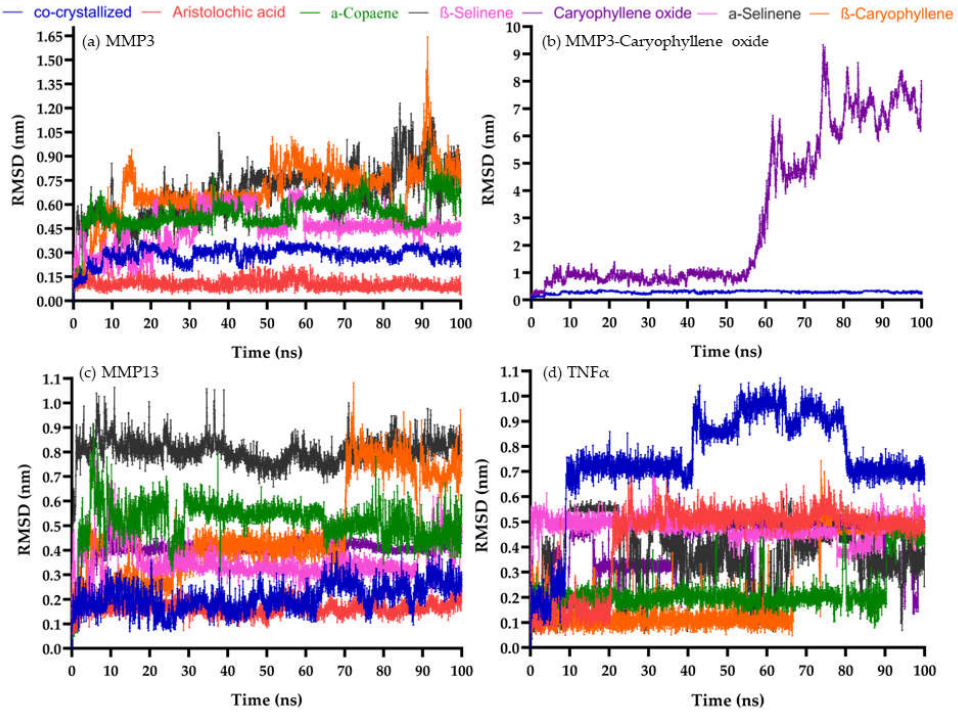

Figure 2. The root-mean-square deviation (RMSD) behavior of selected compounds. (a) MMP-3 pocket (b) MMP-3 pocket, caryophyllene oxide moved out after 50 ns (c) MMP-13 pocket (d) TNFα pocket.

The fact that small molecules such as AA, copaene, selinenes, BC, and BCoxide could serve as MMP-3 or MMP-13 inhibitors is a promising result. MMPs are enzymes synthesized by fibroblasts, keratinocytes, and endothelial and inflammatory cells that normally degrade extracellular and cell-surface proteins including cytokines, chemokines, ECM proteins, cell receptors, and peptides [26]. Elevated protease activity (EPA) by MPPs of cysteine and serine proteases has been demonstrated in the tissue and fluids of human CW in contrast to acute wounds [27,28]. Some MMPs, e.g., gelatinases A and B (MMP-2 and MMP-9), collagenases 1, 2, and 3 (MMP-1, MMP-8, and MMP-13), stromelysin-1 (MMP-3), matrilysin-2 (MMP-26) and a decrease of their endogenous inhibitors (TIMP-1, and TIMP-2) was associated with non-healing CW [25]. The role of the participation of our candidates as MMP-3 or MMP-13 inhibitors is unknown. However, BCoxide contained in *Piper nigrum* induced a decrease

Preprints (www.preprints.org) | NOT PEER-REVIEWED | Posted: 20 April 2023 doi:10.20944/preprints202304.0619.v1

of MMP-9 and MMP-2 release on a fibrosarcoma cell line [29], and BC induced a decrease of MMP-9 and TIMP-1 in the cerebral ischemia-reperfusion injury rat model [29]. and a decrease in elastin degradation and MMP-2 in a nicotine-induced aortic damage mouse model [30]. An interaction of AA with MMP-2 better than their natural inhibitor was also demonstrated in an *in-silico* study [32]. Other natural compounds such as quercetin, luteolin, vicenin-2, and notoginsenoside R1 have been associated with the downregulation of MMP-9, TNFα, IL1β, and IL6, and upregulation of antioxidant enzymes, TIMP, IL10, VEGF, TGFb1, on streptozotocin-induced diabetic rats [33-35]. For MMP-13 (which have essential roles in the turnover of the collagen matrix of bone) natural compounds such as curcumin, resveratrol, and epigallocatechin-3-gallate inhibit the IL-1β or advanced glycation end products-induced production of MMP-13, IL6 or TNFα by chondrocytes [36,37]. Regards the TNFα pocket, AA, and BC showed the best behavior followed by α-copaene and α-selinene, and continuous fluctuations by BCoxide and β-selinene were displayed (Figure 2d). TNFα is one of the major regulators of inflammatory responses and constitutes a therapeutic target in impaired WH [6]. The roles of caryophyllenes (BC and BCoxide) in WH will be described in the next sections.

Aristolochic acid was the best candidate in our *in-silico* study, unfortunately, it was removed from further experimental analysis because of its recognized carcinogenic, mutagenic, and nephrotoxic activities [38]. Nevertheless, it could be an interesting compound as a lead for drug development.

3.3 BC and BCoxide activities on HaCat cells

BC and BCoxide treatment did not affect cell viability of HaCat cells at 300 μg/mL Higher percentages of scratch area closure at 48 h were induced by BC compared with the untreated control (p <0.05) but contrary, no significative effect was induced by BCoxide and allantoin treatment (Figure 3 and Figure S1). The closure caused for the medium plus 10% FCS (p <0.001) was expected and was the reason for to use of culture media supplemented by 1.5% FCS. The proliferative and migrating activities induced by BC have also been demonstrated previously in primary cultured keratinocytes and fibroblasts where higher cell proliferation and migration were observed [39]. Nevertheless, a significant cytotoxicity (CC_{50} from 17 to 45 μg/mL) and reduced cell migration was induced by BC and BCoxide treatment on cancer cells including bladder, epithelial, and prostate tumor cells demonstrating their potential as anticancer agents [25,40].

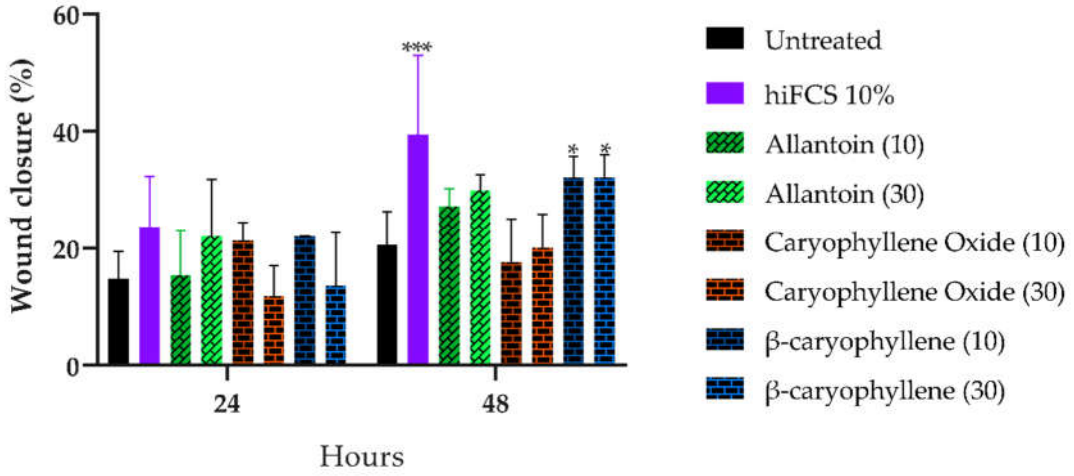

Figure 3. Percentage of scratch area closure induced by BCoxide, BC, and allantoin in HaCat cells at 24 and 48 h. .

Preprints (www.preprints.org) | NOT PEER-REVIEWED | Posted: 20 April 2023 doi:10.20944/preprints202304.0619.v1

3.3 BC and BCoxide activities on BALB/c excisional acute wound model

3.3.1 Initial delay of wound closure was induced by BC and BCoxide treatments.

Based on the lesion area progression along the 10 days of the experiments, the AUCs calculated for allantoin (0.5 and 1%), BCoxide (0.05 and 0.1%), and BC (0.1%) groups were statistically higher than untreated control ($p < 0.001$) (Figure 4a). By day 3, differences in wound closure were observed in almost all experimental groups ($p < 0.001$) being allantoin (0.5 and 1%), BCoxide (0.05, 0.1, and 0.5%), and BC (0.1%) the ones with lower wound closure percentages compared with the untreated or vehicle controls. By the 5th and 8th day, differences were only maintained by BCoxide (0.1%) group ($p < 0.001$). At day 10, similar lesion closure was observed in all groups (Figure 4b). The lesions images are shown in Figure 2S. In contrast to our results, topical treatment with an emulgel containing 1% BC (from *Copaifera langsdorffii* oleoresin), twice a day, 3 doses or a nano emulsified 10% BC hydrogel once a day/7x, 14x induced a faster wound closure than untreated controls on rat excisional models. Those effects were accompanied by the downregulation of proinflammatory cytokines, enhancement of re-epithelization, and antioxidant activities [41,42]. Similar results to those reported here were found with an allantoin emulsion skin treatment, which delayed healing on day 3 compared to the untreated control, but increased fibroblast proliferation and ECM deposition [43].

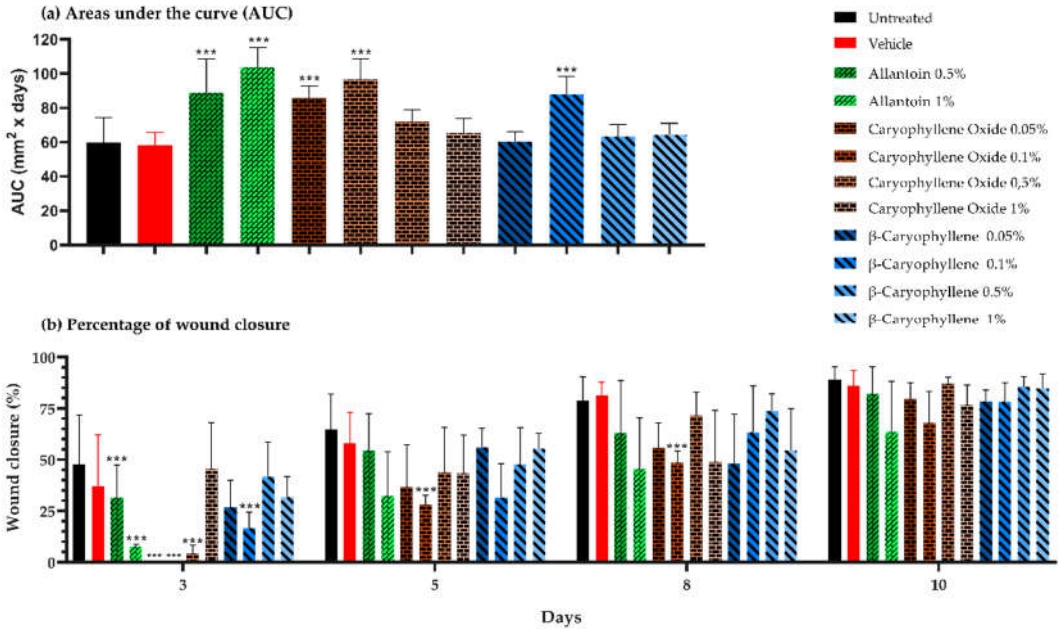

Figure 4. Wound closure induced by topical treatment of PMDs and controls on BALB/c mice excisional wounds (a) Areas under the curve, (b) Percentage of lesion closure at 3, 5, 8, and 10 days of treatment.

3.3.2 Morphometric analysis at the end of treatment

Normal skin images compared with untreated skin showed lower values ($p < 0.05$) of mast cells, cellular infiltrates, and epidermis (without SC) thickness, but similar values of SC thickness were observed in normal skin compared to the untreated skin (Figure 8a).

Comparing the number of mast cells between treated versus untreated groups, BC and BCoxide treatments showed lower numbers of mast cells ($p < 0.05$) (Figure 5a). In the vehicle group, the numbers of cells were similar to the untreated groups. Mast cells by their tissular localization and ability to release diverse classes of mediators (e.g., histamine, tryptases, chymases, VEGF, PDGF, TNFα, TGFβ, IL-1β, IL-6), participated in different WH stages [44]. A dysregulation of mast cells has been related to keloid scar formation. A decrease in mast cells was demonstrated by the epigallocatechin-3-gallate natural compound with a good prognostic in a keloid organ culture model [45]. This could be another interesting role of BC and BCoxide compounds in WH treatment.

Preprints (www.preprints.org) | NOT PEER-REVIEWED | Posted: 20 April 2023 doi:10.20944/preprints202304.0619.v1

In terms of cellular infiltrates and epidermis and SC thickness: i. Lower levels of cellular infiltrates were quantified in all treated groups except 1% BCoxide and 0.05 and 0.5% BC ($p < 0.05$) (Figure 5a); ii. Lesser thickness (no-statistically significant) of the epidermis was quantified in all treatments except by 0.1 and 0.5% BCoxide treatment (figure 5b); and iii. Higher thickness of SC que showed by all treated groups except 0.1 % BCoxide and 0.05 BC treatment ($p < 0.01$) (Figure 5b).

In general, both a no clear dose-response effect, and no complete restoration of the baseline values achieved by normal skin were induced by the BC and BCoxide treatments.

A wide range of biological activities had been linked to BC. BC is considered a potent anti-inflammatory and analgesic compound perhaps by multiple mechanisms, but mostly attributed to its selective binding to the no-psychoactive cannabinoid receptor 2 (CB2) [46]. As a CB2 agonist, it modulates the inflammatory response via the endocannabinoid system and inhibits induced proinflammatory cytokines and edema [46]. C57Bl/6 mice, wounds covered with a BC device induced an increase of several re-epithelialization markers including keratin-14, PDGFRα, filaggrin, and enhancement of keratinocyte and fibroblast proliferation/migration by day 3-4 post-treatment [39].

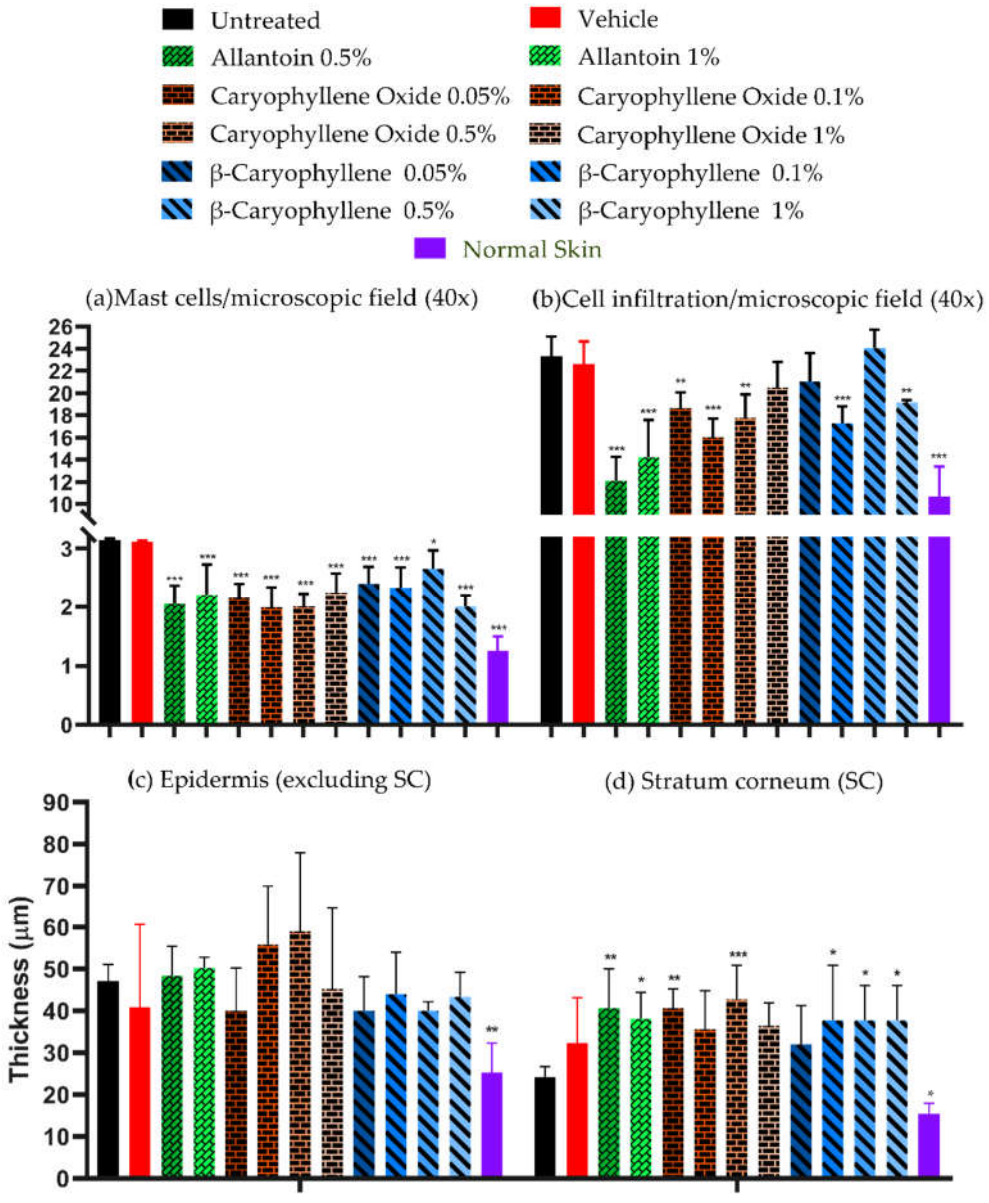

Figure 5. Microscopic image analysis of biopsies at the end of PDMs and controls treatment (a) mast cells and inflammatory infiltrate, and (b) thickness (µm) of the epidermis (excluding SC) and SC, in 300 microscopic fields at 400x magnification.

Preprints (www.preprints.org) | NOT PEER-REVIEWED | Posted: 20 April 2023 doi:10.20944/preprints202304.0619.v1

3.3.3 Collagen deposition in Masson's trichrome-stained slides.

Higher density of collagen fibers in terms of total intensity and several blue pixels per unit area (Figure 6) were displayed by 0.5 and 0.1% BC treatment and by 0.5% BC treatment respectively compared with untreated controls ($p < 0.05$). The higher levels of collagen were similar to those expressed on healthy skin samples (Figure 6, $p < 0.05$). Collagen is a key component of the ECM and plays a critical role in the regulation of the WH process. In a rat model, 1% BC emulgel treatment induced an increase in collagen amount by day 3, but with similar quantities to untreated controls, at 14 days [42]. *In vitro*, BC treatment induced an increase of collagen content differentiate osteoblast cells [47], however in some stimulated cells i.e., high-glucose mesangial cells, or in an HDF3CGF wound healing and inflammation model (BioMAP system), an inhibition of fibronectin and collagen type I, III, or IV were induced by BC or by *Piper nigrum*-EO (BC 21%) treatment [48,49].

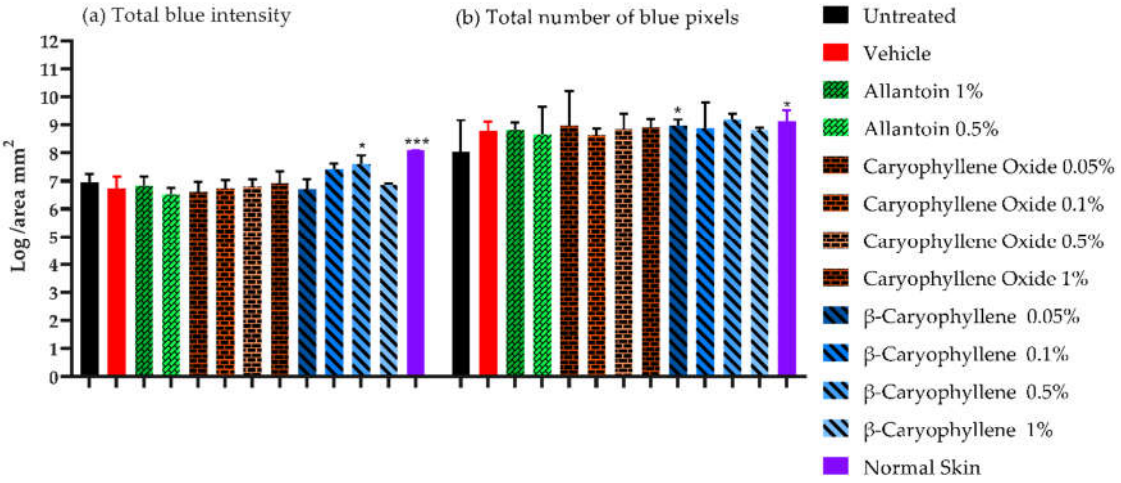

Figure 6. Microscopic image analysis in Masson's trichrome-stained slides at the end of PDMs and controls treatment. The figures showed the logarithm of total intensities and the total number of pixels per area (mm^2).

3.3.4 Tissue-protein and IL-6, IL-1, VEGF and TNFα determination

The cytokine values at 3, 5, and 10 days of treatments are shown in Figure 7. Cytokine levels were higher in infected tissues (treated and untreated) than in normal ones at all evaluated times (except IL-10, day 10). Allantoin was effective in reducing IL-6 levels by day 3 (1%, $p < 0.001$, and 0.5%, $p < 0.01$) but did not affect IL-1, VEGF, and TNF levels. For IL-6 (Figure 7a), values were reduced by day 5 ($p < 0.05$) but they were similar on day 10. A higher IL-6 reduction was induced by 0.5 and 1% BC at day 3 ($p < 0.001$) and 1% BC at day 5 ($p < 0.05$). For IL-1 levels (Figure 7b), a strong reduction was observed by days 5 and 10 ($p < 0.05$) but there were no differences between treated and untreated groups. For VEGF (Figure 7c), the reduction was only observed by day 10 ($p < 0.05$). Interestingly, treatment with 1% BC increased VEGF levels at day 5 ($p < 0.05$). For TNFα (Figure 7d), a decrease was observed by day 10 ($p < 0.05$) without reaching levels similar to healthy skin. A higher TNFα reduction was induced by 1% BC on all days ($p < 0.05$) and 0.5% (days 3 and 5). A decrease in TNFα levels was also induced by 0.1 and 0.5% BCoxide treatment on days 3 and 5 ($p < 0.05$).

Due to the dual property of IL-6 as a pro and anti-inflammatory molecule, the inhibition of IL-6 induced by BC after 3 days could be important for chronic wounds treatment decreasing the deleterious effects of an extensive inflammatory process, but also because its regulation (especially downregulation) as has been demonstrated by some drugs e.g., verapamil, corticosteroid, tocilizumab, improve scar scores in fibrotic and keloid wounds [48]. The increase of VEGF values by BC was also interesting. VEGF is a strong inducer of angiogenesis, and vascular permeability, and a stimulator of endothelial proliferation, migration, differentiation, and survival [49].

For TNFα, a sustained decrease was induced by BC treatment. Like IL-6, TNFα is a pro-inflammatory cytokine and constitutes a therapeutic target in impaired WH [6,37,44]. BC, as we said

Preprints (www.preprints.org) | NOT PEER-REVIEWED | Posted: 20 April 2023 doi:10.20944/preprints202304.0619.v1

before, as an agonist compound (selective) to CB2-receptor, it is a very potent anti-inflammatory molecule [12,44].

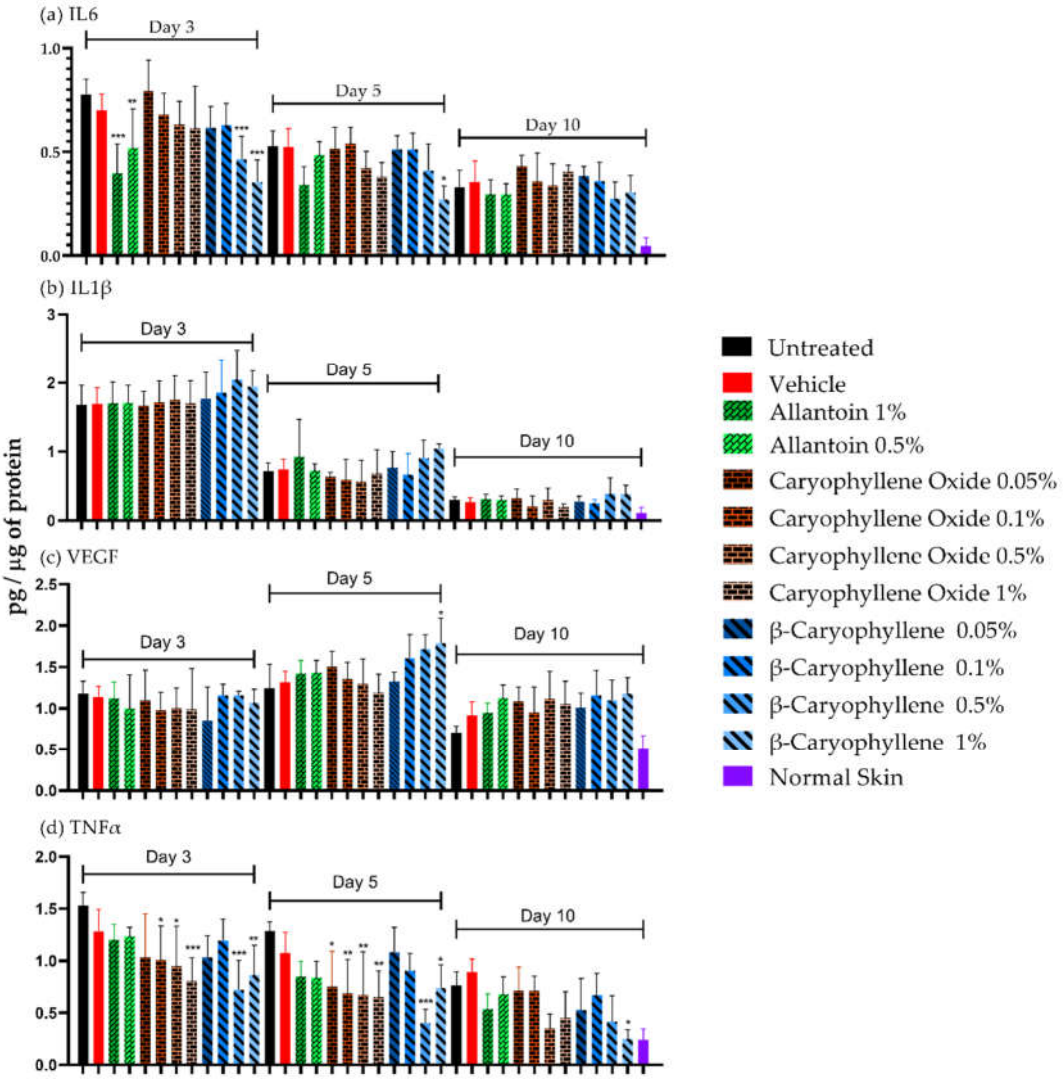

Figure 7. Levels of IL-6, IL-1, VEGF, and TNFα in tissue homogenates (pg/µg protein) for lesions at days 3, 5, and 10 of healing and normal skin.

4. Conclusions

In silico evaluation allows the successful selection of PMDs with pro-healing capacity. Aristolochic acid was the best, however, because its recognized carcinogenic properties were discarded. BC was the most promising candidate. It demonstrates an anti-inflammatory profile (reduction of IL-6 and TNFα; reduction of cellular infiltrate and mast cells), pro-angiogenic (an increase of VEGF), and effects on cell proliferation/migration, re-epithelialization, and collagen deposition. Our results show that BC is a promising multitarget candidate for wound healing treatment and optimization campaigns.

Supplementary Materials: Figure S1: Microphotograph of scratch areas induced by allantoin, caryophyllene oxide, and β-caryophyllene in HaCat cells at 24 and 48 h.; Figure S2: Images of excisional skin lesions in BALB/c mice on different days (0, 5, and 10) for each experimental group; Figure S3: Histological images of excised tissue specimens (thickness 5 µm) with hematoxylin and eosin (H&E), Masson's trichrome, and toluidine blue stained after 10 days for each experimental group.

Author Contributions: Conceptualization, O.C., and P.E.; methodology, formal analysis, and investigation, O.C., O.M., L.G., E.S., J.B.G., J.C.M., P.E.; writing—original draft preparation, O.C., P.E.; writing—review and editing, O.C., O.M., L.G., E.S., J.B.G., J.C.M., P.E.; supervision, project administration, and funding acquisition, P.E. All authors have read and agreed to the published version of the manuscript.

Funding: This research was funded by the Ministry of Science, Technology, and Innovation; the Ministry of Education; the Ministry of Industry, Commerce, and Tourism; ICETEX, the Programme Ecosistema Científico-Colombia Científica; and the Francisco José de Caldas Fund, Grant RC-FP44842-212-2018.

Institutional Review Board Statement: The study was conducted according to the guidelines of the Declaration of Helsinki and approved by the Ethics Committee (CIENCI) of the Industrial University of Santander, Bucaramanga, Colombia (protocol code 4110 and date of approval: May 22, 2022).

Data Availability Statement: Not applicable

Acknowledgments: We would like to thank Heider Carreno, Laura F. Neira, Mary E. Salazar, and Jorge Osorio for their support in some experiments.

Conflicts of Interest: The authors declare no conflicts of interest.

References

1. Gurtner, G.C.; Werner, S.; Barrandon, Y.; Longaker, M.T. Wound repair and regeneration. *Nature* **2008**, *453*, 314-321. doi: 10.1038/nature07039.
2. Guo, S.; Dipietro, L.A. Factors affecting wound healing. *J. Dent. Res.* **2010**, *89*, 219-229. doi: 10.1177/0022034509359125.
3. Smigiel, K.S.; Parks, W.C. Macrophages, wound healing, and fibrosis: recent insights. *Curr. Rheumatol. Rep.* **2018**, *20*, 17. doi: 10.1007/s11926-018-0725-5.
4. Wang, G.; Yang, F.; Zhou, W.; Xiao, N.; Luo, M.; Tang, Z. The initiation of oxidative stress and therapeutic strategies in wound healing. *Biomed. Pharmacother.* **2023**, *157*, 114004. doi: 10.1016/j.biopha.2022.114004.
5. Rodrigues, M.; Kosaric, N.; Bonham, C.A.; Gurtner, G.C. Wound healing: a cellular perspective. *Physiol. Rev.* **2019**, *99*, 665-706. doi: 10.1152/physrev.00067.2017.
6. Ashcroft, G.S.; Jeong, M.J.; Ashworth, J.J.; Hardman, M.; Jin, W.; Moutsopoulos, N.; Wild, T.; McCartney-Francis, N.; Sim, D.; McGrady, G.; Song, X.Y.; Wahl, S.M. Tumor necrosis factor-alpha (TNF-α) is a therapeutic target for impaired cutaneous wound healing. *Wound Repair Regen.* **2012**, *20*, 38-49. doi: 10.1111/j.1524-475X.2011.00748.x.
7. Frykberg, R.G.; Banks, J. Challenges in the treatment of chronic wounds. *Adv. Wound Care* (New Rochelle). **2015**, *4*, 560-582. doi: 10.1089/wound.2015.0635.
8. Yadav, E.; Yadav, P.; Verma, A. *In silico* study of *Trianthema portulacastrum* embedded iron oxide nanoparticles on glycogen synthase kinase-3β: A Possible contributor to its enhanced *in vivo* wound healing potential. *Front Pharmacol.* **2021**, *12*, 664075. doi: 10.3389/fphar.2021.664075.
9. Moses, R.L.; Prescott, T.A.K.; Mas-Claret, E.; Steadman, R.; Moseley, R.; Sloan, A.J. Evidence for natural products as alternative wound-healing therapies. *Biomolecules* **2023**, *13*, 444. doi: 10.3390/biom13030444.
10. Morris, G.M.; Huey, R.; Lindstrom, W.; Sanner, M.F.; Belew, R.K.; Goodsell, D.S.; Olson, A.J. AutoDock4 and AutoDockTools4: Automated docking with selective receptor flexibility. *J. Comput. Chem.* **2009,** 30, 2785-2791. doi: 10.1002/jcc.21256.
11. Amorim, J.L.; Figueiredo, J.B.; Amaral, A.C.F.; Barros, E.G.O.; Palmero, C.; Palantinos, M.A.; Ramos, A.S.; Ferreira, J.LP.; Silva, J.R.A.; Benjamim, C.F.; Basso, S.L.; Nasciutti, L.E.; Fernandes, P.D. Wound healing properties of *Copaifera paupera* in diabetic mice. PLoS One **2017**, *12*, e0187380. doi: 10.1371/journal.pone.0187380.
12. Sousa Da Silva, A.W.; Vranken, W.F. ACPYPE-AnteChamber PYthon Parser interfacE. BMC Research Notes, **2012**, *5*, 1–8. https://doi.org/10.1186/1756-0500-5-367
13. Rosenthal, M.D.; Vishwanath, B.S.; Franson, R.C. Effects of aristolochic acid on phospholipase A2 activity and arachidonate metabolism of human neutrophils. *Biochim. Biophys, Acta* **1989**, *23*, 1-8. doi: 10.1016/0005-2760(89)90299-3.

14. Murugan, D.; Mangathayaru, K.; Rajasekaran, S.; Preeth, J.; Rangarao, S. *Aristolochia bracteolata* enhances wound healing through anti-inflammatory and proliferative effect on human dermal fibroblasts and keratinocytes. *Pharmacogn. J.* **2017**, *9*. 129-136. doi: 10.5530/pj.2017.6s.169.
15. Bolla, S.R.; Mohammed Al-Subaie, A.; Yousuf Al-Jindan, R.; Papayya Balakrishna, J.; Kanchi, Ravi, P.; Veeraraghavan, V.P.; Arumugam Pillai, A.; Gollapalli, S.S.R.; Palpath Joseph, J.; Surapaneni,. K.M. *In vitro* wound healing potency of methanolic leaf extract of *Aristolochia saccata* is possibly mediated by its stimulatory effect on collagen-1 expression. *Heliyon* **2019**, 5, e01648. doi: 10.1016/j.heliyon.2019.e01648.
16. Shirwaikar, A.; Somashekar, A.P.; Udupa, A.L.; Udupa, S.L.; Somashekar, S. Wound healing studies of *Aristolochia bracteolata* Lam. with supportive action of antioxidant enzymes. *Phytomedicine* **2003**, 10, 558-562. doi: 10.1078/094471103322331548.
17. Souza, B.E.; Ottoni, M.H.F.; de Alvarenga, P.G.M.; Meireles, A.B.; Silveira, J.V.W.; Almeida, V.G.; Dos Santos, M.G.; González-Torres, L.A.; Fuzer Grael, C.F.; Alvim Brito-Melo, G.E.; Avelar-Freitas, B.A. Effect of essential oil from *Ageratum fastigiatum* on beta-integrin (CD18) expression on human lymphocytes stimulated with phorbol myristate acetate *in vitro*. *Nat. Prod. Res*. **2020**, *34*, 3409-3413. doi: 10.1080/14786419.2019.1569653
18. Seyed Ahmadi, S.G.; Farahpour, M.R.; Hamishehkar ,H. Topical application of *Cinnamon verum* essential oil accelerates infected wound healing process by increasing tissue antioxidant capacity and keratin biosynthesis. *Kaohsiung J. Med. Sci*. **2019**, *35*, 686-694. doi: 10.1002/kjm2.12120.
19. Soares, K.D.; Bordignon, S.A.L.; Apel, M.A. Chemical composition and anti-inflammatory activity of the essential oils of *Piper gaudichaudianum* and *Piper mikanianum*. *J. Ethnopharmacol*. **2022**, *297*, 115533. doi: 10.1016/j.jep.2022.115533.
20. Andjić, M.; Božin, B.; Draginić, N.; Kočović, A.; Jeremić, J.N.; Tomović, M.; Milojević Šamanović, A.; Kladar, N.; Čapo, I.; Jakovljević, V.; Bradić, J.V. Formulation and evaluation of *Helichrysum italicum* essential oil-based topical formulations for wound healing in diabetic rats. *Pharmaceuticals* **2021,** 14, 813. https://doi.org/10.3390/ph14080813
21. Perini, J.A.; Angeli-Gamba, T.; Alessandra-Perini, J.; Ferreira, L.C.; Nasciutti, L.E.; Machado, D.E. Topical application of Acheflan on rat skin injury accelerates wound healing: a histopathological.; immunohistochemical and biochemical study. *BMC Complement Altern. Med*. **2015**, *15*, 203. doi: 10.1186/s12906-015-0745-x.
22. Mazutti da Silva, S.M.; Rezende Costa, C.R.; Martins Gelfuso, G.; Silva Guerra, E.N.; de Medeiros Nóbrega, Y.K.; Gomes, S.M.; Pic-Taylor, A.; Fonseca-Bazzo, Y.M.; Silveira, D.; Magalhães, P.O. Wound healing effect of essential oil extracted from *Eugenia dysenterica* DC (Myrtaceae) leaves. *Molecules*. **2018**, 24, 2. doi: 10.3390/molecules24010002.
23. Fidyt, K.; Fiedorowicz, A.; Strządała, L.; Szumny, A. β-caryophyllene and β-caryophyllene oxide-natural compounds of anticancer and analgesic properties. *Cancer Med*. **2016**, 10, 3007-3017. doi: 10.1002/cam4.816.
24. Parks, W.C.; Wilson, C.L.; López-Boado, Y.S. Matrix metalloproteinases as modulators of inflammation and innate immunity. *Nat. Rev. Immunol*. **2004**, *8*, 617-629. doi: 10.1038/nri1418.
25. Lazaro, J.L.; Izzo, V.; Meaume, S.; Davies, A.H.; Lobmann, R.; Uccioli, L. Elevated levels of matrix metalloproteinases and chronic wound healing: an updated review of clinical evidence. *J. Wound Care* **2016**, 25, 277-287. doi: 10.12968/jowc.2016.25.5.277.
26. Lockmann, A.; Schill T.; Hartmann, F.; Grönemeyer, L.L.; Holzkamp, R.; Schön, M.P.; Thoms, K.M. Testing elevated protease activity: prospective analysis of 160 wounds. *Adv. Skin Wound Care*. **2018**, *31*, 82-88. doi: 10.1097/01.ASW.0000527965.64870.03.
27. Jo, H.W.; Kim, M.M. β-Caryophyllene oxide inhibits metastasis by downregulating MMP-2, p-p38 and p-ERK in human fibrosarcoma cells. *J. Food Biochem*. **2022,** *46*, e14468. doi: 10.1111/jfbc.14468.
28. Liu, S.; Liu, J.; Wang, Y.; Deng, L.; Chen, S.; Wang, X.; Zuo,T.; Hu, Q.; Rao, J.; Wang, Q.; Dong, Z. Differentially expressed genes induced by β-caryophyllene in a rat model of cerebral ischemia-reperfusion injury. *Life Sci*. **2021**, *273*, 119293. doi: 10.1016/j.lfs.2021.119293.
29. Kishi, C.; Higashihara, M.; Takemoto, Y.; Kamei, M.; Yoshioka, Y.; Matsumura, S.; Yamada, K.; Kobayashi, T.; Matahira, Y.; Moriyama, T.; Zaima, N. Inhaled volatile β-caryophyllene is incorporated into the aortic wall and attenuates nicotine-induced aorta degeneration via a CB2 receptor-dependent pathway. *Biomed. Pharmacother*. **2022**, *153*, 113423. doi: 10.1016/j.biopha.2022.113423
30. Fathima, J.S.; Selvaraj, J.; Sivabalan, V.; Rekha, U.V.; Ponnulakshmi, R.; Vishnupriya, V.; Kullappan, M.; Sreekandan, R.N.; Mohan, S.K. Molecular docking of alkaloid compounds with the matrix metalloproteinase 2. *Bioinformation* **2021**, *17*, 206-211. doi: 10.6026/97320630017206.
31. Kant, V.; Jangir, B.L.; Sharma, M.; Kumar, V.; Joshi, V.G. Topical application of quercetin improves wound repair and regeneration in diabetic rats. *Immunopharmacol. Immunotoxicol*. **2021**, *43*, 536-553. doi: 10.1080/08923973.2021.1950758.
32. Chen, L.Y.; Cheng, H.L.; Kuan, Y.H.; Liang, T.J.; Chao, Y.Y.; Lin, H.C. Therapeutic potential of luteolin on impaired wound healing in streptozotocin-induced rats. *Biomedicines* **2021**, *9*, 761. doi: 10.3390/biomedicines9070761.

33. Cao, G.; Xiang, C.; Zhou, R.; Zhang, Y.; Xu, H.; Yang, H.; Zhang, J. Notoginsenoside R1 facilitated wound healing in high-fat diet/streptozotocin-induced diabetic rats. *Oxid. Med. Cell. Longev*. **2022** Jan 13;2022:2476493. doi: 10.1155/2022/2476493.
34. Yang, Q.; Wu, S.; Mao, X.; Wang, W.; Tai, H. Inhibition effect of curcumin on TNF-α and MMP-13 expression induced by advanced glycation end products in chondrocytes. *Pharmacology* **2013**, *91*, 77-85. doi: 10.1159/000345345.
35. Gu, H.; Jiao, Y.; Yu, X.; Li, X.; Wang, W.; Ding, L.; Liu, L. Resveratrol inhibits the IL-1β-induced expression of MMP-13 and IL-6 in human articular chondrocytes via TLR4/MyD88-dependent and -independent signaling cascades. *Int. J. Mol. Med.* **2017**, *39*, 734-740. doi: 10.3892/ijmm.2017.2885.
36. Han, J.; Xian, Z.; Zhang, Y.; Liu, J.; Liang, A. Systematic overview of aristolochic acids: nephrotoxicity., carcinogenicity, and underlying mechanisms. *Front. Pharmacol*. **2019**, 10, 648. doi: 10.3389/fphar.2019.00648.
37. Koyama, S.; Purk, A.; Kaur, M.; Soini, H.A.; Novotny, M.V.; Davis, K.; Kao, C.C.; Matsunami, H.; Mescher, A. Beta-caryophyllene enhances wound healing through multiple routes. PLoS One. **2019**, *14*, e0216104. doi: 10.1371/journal.pone.0216104.
38. Delgado C, Mendez-Callejas G.; Celis C. Caryophyllene oxide, the active compound isolated from leaves of *Hymenaea courbaril* L. (Fabaceae) with antiproliferative and apoptotic effects on pc-3 androgen-independent prostate cancer cell line. Molecules. **2021** Oct 12;26(20):6142. doi: 10.3390/molecules26206142.
39. Parisotto-Peterle, J.; Bidone, J.; Lucca, L.G.; Araújo, G.M.S.; Falkembach, M.C.; da Silva Marques, M.; Horn, A.P.; Dos Santos, M.K.; da Veiga, V.F. Jr.; Limberger, R.P.; Teixeira, H.F.; Dora, C.L.; Koester, L.S. Healing activity of hydrogel containing nanoemulsified β-caryophyllene. *Eur. J. Pharm. Sci*. **2020**, *148*, 105318. doi: 10.1016/j.ejps.2020.105318.
40. Gushiken, L.F.S.; Beserra, F.P.; Hussni, M.F.; Gonzaga, M.T.; Ribeiro, V.P.; de Souza, P.F.; Campos, J.C.L.; Massaro, T.N.C.; Hussni, C.A.; Takahira, R.K.; Marcato, P.D.; Bastos, J.K.; Pellizzon, C.H. Beta-caryophyllene as an antioxidant, anti-inflammatory and re-epithelialization activities in a rat skin wound excision model. *Oxid. Med. Cell. Longev*. **2022**, *2022*, 9004014. doi: 10.1155/2022/9004014.
41. Araújo, L. U.; Grabe-Guimarães, A.; Mosqueira, V.C.F.; Carneiro, C.M.; Silva-Barcellos, N.M. Profile of wound healing process induced by allantoin. *Acta Cir. Bras*. **2010**, *25*, 460–466. https://doi.org/10.1590/s0102-86502010000500014
42. Komi, D.E.A.; Khomtchouk, K.; Santa Maria, P.L. A review of the contribution of mast cells in wound healing: involved molecular and cellular mechanisms. *Clin. Rev. Allergy. Immunol*. **2020**, *58*, 298-312. doi: 10.1007/s12016-019-08729-w.
43. Syed, F.; Bagabir, R.A.; Paus, R.; Bayat, A. *Ex vivo* evaluation of antifibrotic compounds in skin scarring: EGCG and silencing of PAI-1 independently inhibit growth and induce keloid shrinkage. *Lab. Invest*. **2013**, *93*, 946-960. doi: 10.1038/labinvest.2013.82.
44. Gertsch, J.; Leonti, M.; Raduner, S.; Racz, I.; Chen, J.Z.; Xie, X.Q.; Altmann, K.H.; Karsak, M..; Zimmer, A. Beta-caryophyllene is a dietary cannabinoid. *Proc. Natl. Acad. Sci. USA*. **2008**, *105*, 9099–9104. doi: 10.1073/pnas.0803601105
45. Shan, J.; Chen, L.; Lu, K. Protective effects of trans-caryophyllene on maintaining osteoblast function. *IUBMB Life*. **2017**, *69*, 22-29. doi: 10.1002/iub.1584. PMID: 28026135.
46. Han, X.; Beaumont, C.; Rodriguez, D.; Bahr, T. Black pepper (*Piper nigrum*) essential oil demonstrates tissue remodeling and metabolism modulating potential in human cells. *Phytother. Res*. **2018**, *32*, 1848-1852. doi: 10.1002/ptr.6110.
47. Li, H.; Wang, D.; Chen, Y.; Yang, M. β-Caryophyllene inhibits high glucose-induced oxidative stress, inflammation and extracellular matrix accumulation in mesangial cells. *Int. Immunopharmacol*. **2020**, *84*, 106556. doi: 10.1016/j.intimp.2020.106556.
48. Johnson, B.Z.; Stevenson, A.W.; Prêle, C.M.; Fear, M.W.; Wood, F.M. The role of IL-6 in skin fibrosis and cutaneous wound healing. *Biomedicines* **2020**, *8*. https://doi.org/10.3390/biomedicines8050101
49. Leung, D.W.; Cachianes, G.; Kuang, W.J.; Goeddel, D.V.; Ferrara, N. (1989). Vascular endothelial growth factor is a secreted angiogenic mitogen. *Science* **1989**, 246,, 1306–1309. https://doi.org/10.1126/science.2479986